Contrib Mineral Petrol (1992) 112:371–384

Contributions to Mineralogy and Petrology

Modeling of the transport and deposition of tungsten in the scheelite-bearing calc-silicate gneisses of the Montagne Noire, France

François Gibert, Bernard Moine, Jacques Schott, and Jean-Louis Dandurand

Laboratoires de Minéralogie et de Géochimie, UA 067 du CNRS, Université Paul Sabatier, 39, allées Jules Guesde, F-31000 Toulouse, France

Received November 21, 1991/Accepted April 24, 1992

Abstract. Scheelite-bearing calc-silicate gneisses (CSG) occur in the Montagne Noire within a series of dominant micaschists. Detailed petrographical and mineralogical studies reveal three successive stages of metamorphism and hydrothermal alteration: (1) stage 1, a regional metamorphism at 550 °C and 4.5 kb where no mineralization is formed; (2) stage 2a, a hydrothermal alteration at 500 to 450 °C and 4 to 3 kb which is characterized by an intense sericitization of feldpars and deposition of Sn in Sn-bearing calc-silicates; and (3) stage 2b, a hydrothermal alteration characterized by the crystallization of idocrase-grossular in CSG with concomittant precipitation of scheelite. Tungsten was transported through the micaschist environment and deposited as scheelite only in the CSG of stage 2b at relatively low pressures. To characterize the mechanism of tungsten transport, tungsten speciation at high P-T and scheelite solubility in aqueous solutions buffered by the CSG and by the micaschists assemblages were calculated. It was found that $H_2WO_4^0$, HWO_4^- and WO_4^{2-} are the dominant tungsten aqueous species in H_2O-NaCl (one molal) solutions at 500 °C and 2–4 kb. Calculations also indicate that scheelite deposition is controlled by decreasing pressure and increasing activity of aqueous calcium in this system. This is consistent with the petrographical and mineralogical observations. The consequences of the presence of volatiles (N_2, CH_4, CO_2) in the regional fluids were examined by determining the effect of N_2 on tungsten speciation and scheelite solubility. The addition of N_2 (up to 10 mol %) to the mineralizing fluids results in a marked increase in $H_2WO_4^0$ and HWO_4^- concentrations relative to WO_4^{2-} and in a large decrease of scheelite solubility. This mechanism favours scheelite precipitation and accounts for the commonly observed association of W (and Sn) deposits with graphitic series generating mixed volatiles fluids.

Introduction

Tungsten concentrations commonly occur as stratiform scheelite ($CaWO_4$)-bearing calc-silicate gneisses (CSG) within series of schists and aluminous gneisses and do not show any direct connection with granitic plutonism. These tungsten concentrations have been interpreted as being of sedimentary-exhalative origin (Boyer and Routhier 1974; Plimer 1980, 1987; Fulp and Renshaw 1985; Ririe 1989; see also a detailed review by Cheilletz 1988). However, detailed petrological and geochemical studies have demonstrated that in most cases the host CSG has been metasomatized by reactions with infiltrating fluids and that the tungsten concentrations were closely related to this metamorphic-hydrothermal episode (Tweto 1960; Derré et al. 1982; Cheilletz 1983; Zahm 1987; De Smedt and Sonnet 1988; Gibert et al. 1988, Gibert et al. 1989). This petrological interpretation implies that tungsten would have been transported by fluids circulating through aluminous rocks and deposited as scheelite in the calc-silicate gneisses under metamorphic conditions.

A priori it is likely that a major cause for scheelite precipitation is the increase of calcium activity resulting from the chemical equilibration of the mineralizing fluid with the CSG host rocks, however, other physical and chemical parameters could also play an important role in scheelite deposition. For example, scheelite solubility in aqueous solutions of NaCl falls by a factor of 4-5 when temperature decreases from 450 to 300 °C and it also decreases when NaCl concentration is reduced (see detailed calculations in Rafal'skiy et al. 1984). Pressure is probably another important parameter controlling scheelite deposition. However, to the best of our knowledge, it has never been investigated. In addition, microthermometric studies and Raman spectroscopy analyses of fluid inclusions have shown that W-Sn mineralizing fluids often exhibit relatively high concentrations of non-polar volatiles such as CO_2, CH_4 and N_2 (Dubessy et al. 1987) whose effect on transport and deposition of tungsten has never been quantified.

A detailed petrological and mineralogical study was carried out to determine the P-T-X_{CO_2} conditions of crystallization for the successive stages of the metamorphic/hydrothermal history and the chemical compositions of the aqueous solutions in equilibrium with the different parageneses. Using these data various calculations were performed to evaluate the respective roles of

Correspondence to: F. Gibert

temperature, pressure and fluid composition, including nonpolar volatile content, on the transport of tungsten and its deposition as scheelite. The purpose of this paper is to describe the role of different physical and chemical parameters on the transport and deposition of tungsten by focusing on the example of the W-Sn bearing CSG of the Montagne Noire.

Regional geological setting

The Montagne Noire is located at the southern edge of the Massif Central and is comprised of three main tectonic units: the northern slope, the southern slope and the Axial Zone (sensu lato) (Fig. 1; Thoral 1935; Gèze 1949).

The northern and the southern slopes of the Montagne Noire consist of epimetamorphic Paleozoic rocks. The southern slope is composed of allochtonous units separated from the Axial Zone (sensu lato) basement by a major thrust fault formed during the Hercynian phase of deformation D1 (recumbent isoclinal folding: Arthaud 1970). The D2 deformation (upright refolding) is synchronous with the uplift of the Axial Zone (sensu lato).

The Axial Zone (sensu lato) is comprised of two distinct lithological units (Demange 1982): (1) a basement composed of orthogneisses and migmatites with some interlayers of paragneisses (hereafter referred to as the Axial Zone), and (2) its cover, composed of medium-grade metamorphic rocks, mainly porphyroblastic schists and metagreywackes with some graphitic schists, quartzites and calc-silicate bearing gneisses (hereafter referred to as the Schistes X) which are probably Cambro-Ordovician in age. These rocks are characterized by a polyphased metamorphic history with two major stages (Demange 1982, 1985). The first stage is a metamorphism of intermediate- to low-pressure type and related to the D1 deformation. The second stage is a low pressure type metamorphism, concomitant with the uplift of the orthogneissic dome.

Calc-silicate gneisses occur within two different structural units of the Montagne Noire. The first occurs within the Axial Zone in association with paragneisses levels. The second, which contains most of the mineralized CSG (up to 1% W and 2000 ppm Sn), and thus the bulk of the W and Sn in this system, is located in the lower part of the "Schistes X" series. The CSG are observed along seventy kilometers (from Cabardès to Lamalou, Fig. 1) as stratiform lenticular levels (0.x m thick) interlayered with staurolite-garnet micaschists and black schists.

Two generations of pegmatitic veins are observed in the Schistes X series. The older ones, which are sub-horizontal (post D1–ante D2), usually contain cassiterite (up to 3000 ppm of Sn). The second generation (post D2) is sub-vertical and does not contain cassiterite. Cassiterite has also been discovered in a quartz-tourmaline subvertical vein structure (post D2; Gibert 1991). No significant W mineralization has been observed in these pegmatitic veins.

The lack of connection between the W (Sn) mineralized CSG and any granitic stock, as well as the large extension of the CSG bodies, have been previously interpreted as evidence for a sedimentary-exhalative origin of the tungsten anomalies (Boyer and Routhier 1974).

Petrology and mineralogy of the calc-silicate gneisses

Two main stages of crystallization have been identified in the calc-silicate gneisses of the Schistes X series (Gibert 1991).

Stage 1. regional metamorphism

The earliest preserved crystallization stage (1) results from the regional metamorphism and is characterized by a main paragenesis

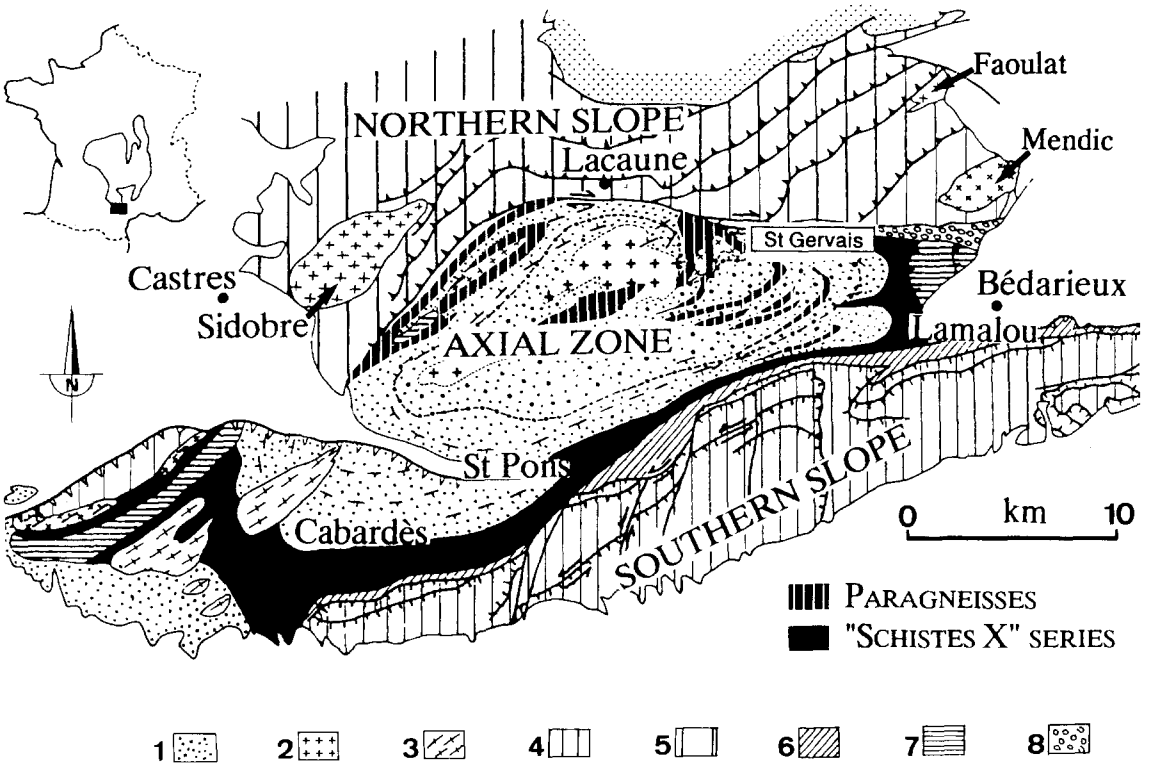

Fig. 1. Geological sketch map of the Montagne Noire 1: Migmatites and orthogneisses; 2: Hercynian granites; 3: deformed Hercynian granites; 4: Cambro-Ordovician (southern slope); 5: Cambro-Silurian (northern slope); 6: Devonian (southern slope); 7: Cambrian; 8: Stephanian

Table 1. Mineral assemblages, pressures, temperatures and mole fractions of CO_2 characteristic of the different stages of metamorphism and alteration of the calc-silicate gneisses

Main stage of metamorphism Stage 1	Late metamorphism hydrothermal alteration Stage 2a	Stage 2b
Clinopyroxene (Hd45-50)	Sericite	Idocrase
Plagioclase (An90)	Cpx (Hd40-50)	Grossular
K-Feldspar	Czo (Ps10, Sn)	Czo (Ps15, Sn)
Clinozoisite (Ps10)	Titanite	Scheelite
Titanite	(12% Al_2O_3, Sn)	Fluorite
(2% Al_2O_3)	Malayaite	Sericite
Quartz	Quartz	Quartz
	Plagioclase (An40)	{Plagioclase}
	{K-Feldspar}	{Cpx}
4.5 kb, 550 °C	4 kb, 500 °C	2 kb, 500 °C
$XCO_2 < 0.16$	to 3 kb, 450 °C	$XCO_2 < 0.01$
	$XCO_2 < 0.03$	

Abbreviations: Cpx = Clinopyroxene; Hd = Hedenbergite; An = Anorthite; Ps = Pistacite; Czo = Clinozoisite; {relic mineral}

consisting of clinozoisite, clinopyroxene, plagioclase, K-feldspar, quartz, and titanite. Clinozoisite is the most widespread of the CSG minerals in the Schistes X series. Its composition is close to Ps10 (see abbreviations in Table 1). Thin section observations suggest that, in this stage, clinozoisite is in equilibrium with K-feldspar and calcic plagioclase (An90). Clinopyroxene composition does not vary significantly (Di45-Hd55). The proportion of quartz is quite variable, but it is always present in the CSG. Titanite is also frequently encountered in these rocks and exhibits low Al_2O_3 concentrations (2 to 4 wt%). The CSG of the Axial Zone show a similar mineralogical association except that epidote is replaced by a Na-K pargasite.

Stage 2, hydrothermal alteration event

The first stage of crystallization is followed by an important hydrothermal alteration of stage 1 minerals. It comprises two separate episodes. The first (stage 2a) is a retrograde process characterized by an intense sericitization of the feldspars and the crystallization of Sn-bearing calc-silicates (Table 1).Titanite formed at this stage contains up to 12 wt% Al_2O_3 (42 mol % of vuagnatite and fluor-vuagnatite) and is chemically homogeneous (Gibert et al. 1990). The second episode of hydrothermal alteration (stage 2b) is characterized by the overgrowth of porphyroblastic idocrase and grossular ± clinozoisite (Table 1). Some of these idocrase grossular-bearing rocks show relatively high calcium concentrations (Fig. 2; Table 2, analyses M16 and 13BM) due to carbonate-rich precursors or to addition of Ca in the course of the alteration. This stage ended or was followed by a minor stage of fluorite crystallization. The W mineralization, as scheelite, occurs only at stage 2b.

Whole-rock geochemistry

Numerous chemical analyses (major and trace elements) of the different metamorphic rocks have been carried out to determine the nature of the protoliths and to quantitatively characterize the metasomatic alteration (Gibert et al. 1988; Gibert 1991). These studies indicate that stage 1 CSG originated from isochemical metamorphism of calcareous pelites and sandstones, the composition of which was consistent with that of the whole series (see Fig. 2 and Table 2). A geochemical comparison with the northern slope of the Montagne Noire suggests that the Schistes X series should be the stratigraphical equivalent, at higher metamorphic conditions, of the lower Cambrian "black schists formation" (Caleffi et al. 1988). In

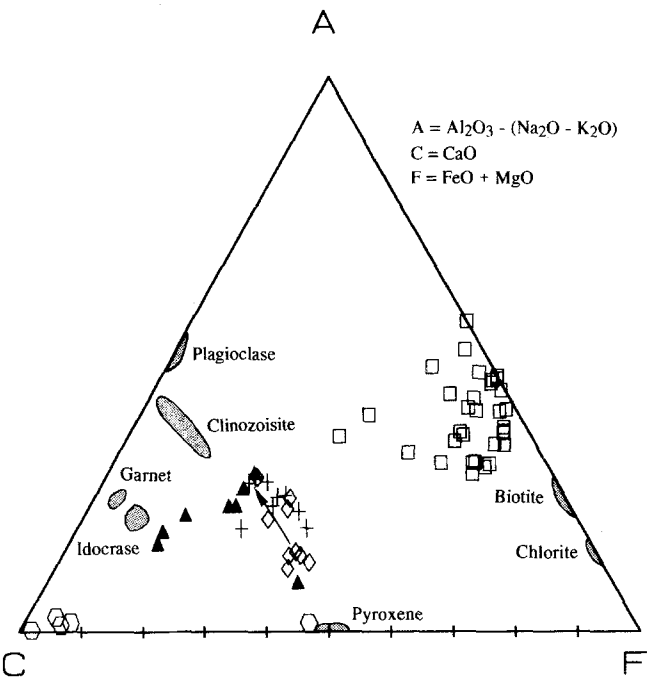

Fig. 2. ACF plot of the different rock and mineral compositions. *Squares* and *hexagons* represent the micaschists and the marbles, respectively. *Diamonds, crosses* and *triangles* represent stage 1, stage 2a and stage 2b CSG, respectively. Microprobe analyses of the minerals plot in the *grey areas*

addition, it has been shown that stage 2 CSG resulted from the metasomatic alteration of the stage 1 CSG through an intense leaching of alkalis (stage 2a; see Table 2 and Fig. 2) and a small addition of Al (stage 2b). Note that no traces of this alteration episode can be found in the CSG of the Axial Zone.

Another important feature is the absence of W (Sn) anomalies in the CSG of stage 1 found in the Schistes X series or in the Axial Zone (< 6 ppm) as well as in the surrounding rocks (< 4 ppm in paragneisses, micaschists and black schists). In addition to the petrographical observations this demonstrates that the Sn-W mineralizations in the CSG of the Montagne Noire did not originate from exhalative sedimentary processes, but were formed during the second stage of metamorphism.

P-T-X conditions

The P-T-X_{CO_2} conditions of metamorphism and hydrothermal alteration can be constrained from phase mineral equilibria using the internally-consistent thermodynamic data set of Berman (1988), and the Geo-Calc computer program (Berman et al. 1987; Brown et al. 1989). In the calculations, the actual mineral compositions obtained from microprobe analyses were taken into account within the framework of the following solid solution models. The activities of epidote and clinozoisite in the epidote solid solution and activity of grossular in garnet were calculated according to equations and parameters reported by Bird and Helgeson (1980). The activities of anorthite and albite in plagioclase were computed using the Newton et al. (1981) model. Muscovite activity in white mica was obtained using the ideal site mixing model (Powell 1978). The activities of the end-members in clinopyroxene, titanite and K-feldspar were estimated to be equal to their mole fraction. The activities of H_2O and CO_2 in H_2O-CO_2 mixtures were calculated using the Redlich Kwong equation modified by Kerrick and Jacobs (1981).

The maximum temperature reached during stage 1 was estimated by applying garnet-biotite geothermometers to the "Schistes X" micaschists surrounding the CSG. A temperature of about 550 °C

Table 2. Chemical analyses representative of the micaschists and of the different calc-silicate gneisses. Major oxides in percent; minor elements in ppm; LOI = loss on ignition

	Micaschists			Calc-silicates gneisses									
				Stage 1			Stage 2a				Stage 2b		
	X24	38	333	L17A	E4	13BS	E10	K27	K11	21	K6	M16	13BM
SiO_2	59.09	62.86	63.94	62.06	54.48	53.84	57.52	57.65	56.66	55.53	56.76	43.70	39.08
Al_2O_3	18.63	17.55	18.34	11.97	16.74	12.77	12.98	14.64	16.48	16.37	17.55	18.75	17.03
Fe_2O_3	6.96	5.93	4.95	4.11	6.58	6.75	5.87	5.03	5.07	6.24	4.79	3.97	3.87
MnO	0.05	0.09	0.03	0.05	0.11	0.09	0.20	0.15	0.09	0.11	0.11	0.17	0.12
MgO	3.12	2.02	2.00	3.92	3.10	5.05	4.27	3.59	2.84	3.02	2.07	2.82	2.49
CaO	0.61	1.02	0.39	9.73	12.63	14.73	12.25	11.10	11.85	13.95	12.75	26.10	30.18
Na_2O	1.43	2.16	0.82	2.18	1.05	1.97	0.63	0.76	2.45	1.82	1.33	0.70	0.90
K_2O	5.66	3.75	4.13	3.37	2.34	1.68	2.32	3.18	1.03	1.18	1.29	1.39	0.74
TiO_2	0.92	0.86	0.98	0.50	0.76	0.81	0.70	0.69	0.56	0.82	0.65	0.36	0.26
P_2O_5	0.25	0.30	0.45	0.20	0.22	0.49	0.92	0.32	0.38	0.35	0.25	0.22	0.45
LOI	2.5	2.19	4.38	1.48	1.19	1.25	2.06	2.53	2.21	0.80	2.08	2.04	4.57
Total	99.22	98.73	100.41	99.57	99.20	99.43	99.72	99.64	99.62	100.19	99.63	100.22	99.69
Ba	548	594	1002	649	472	1709	127	356	229	413	88	288	257
Be	–	–	–	1	–	15	–	16	16	–	51	181	97
Co	13	15	12	30	27	26	27	30	30	35	30	9	20
Cr	99	91	115	58	95	155	88	97	82	105	89	51	86
Cu	11	171	20	> 10	22	14	> 10	13	20	62	29	> 10	> 10
Nb	–	–	–	30	15	23	14	30	30	–	30	10	5
Ni	35	43	38	30	58	93	62	47	53	64	31	20	27
Rb	209	129	136	108	78	68	91	128	46	41	53	51	37
Sc	–	–	–	11	–	22	–	14	14	–	16	10	14
Sr	217	164	47	525	764	2787	429	493	826	1354	703	583	947
V	205	129	141	79	141	169	151	202	108	147	155	115	273
Y	–	–	–	28	32	40	51	32	55	–	36	20	25
Zn	–	–	–	69	0	190	0	87	68	–	79	91	123
Zr	–	–	–	248	160	173	188	200	158	–	206	89	54
W	3	2	2	2	5	3	13	13	3	7	443	3400	9700
Sn	–	–	–	5	7	–	239	134	86	–	554	1276	530

Major oxides and elements Ba to Zr analyzed in Centre de Recherches Pétrographiques et Géochimiques (Nancy) by ICP. W and Sn analyzed in Laboratoire de Géochimie (Toulouse) by colorimetry and atomic absorption, respectively.

was obtained using several geothermometers (Indares and Martignole 1985; Perchuck and Lavrent'eva, 1983; Hoinkes 1986). Figure 3 shows the calculated P-X_{CO_2} section for the system Ca-Al-Si-K-Ti-O-H-C at T = 550 °C. The reactions (1) to (25) considered in Figs. 3 and 4 are given in Table 3. The reactions delimiting the stability field of stage 1 mineral assemblage are (abbreviations as in Table 3):

$$2Zo + CO_2 = Cc + 3An + H_2O \quad (12)$$

$$aQz + 2Cc + An = Gr + 2CO_2 \quad (4)$$

$$2Zo + 2aQz + Ms = 4An + Kfs + 2H_2O \quad (14)$$

It can be seen that total pressure (3.3 kb < P < 5 kb) and X_{CO_2} ($0 < X_{CO_2} < 0.16$) are constrained by the observed mineral assemblage. However, the actual pressure was probably near the upper limit of this range (4.5-5 kb) as indicated by the local occurrence of kyanite in the region (Bouchardon et al. 1979; Demange 1982, 1985; Demange et al. 1986). These P-T conditions are consistent with the presence of staurolite, biotite and garnet in the surrounding micaschists and with the present interpretation of the Montagne Noire geology (Arthaud 1970; Demange 1982).

The P-T conditions of stage 2a can be seen in Fig. 4. All the equilibria involving plagioclases in this P-T diagram were recalculated using the activity model of Newton et al. (1981) because there is no provision for the calculation of the activity of plagioclase in the Geo-Calc program (Berman et al. 1987). As opposed to epidote solid solutions where the activity of clinozoisite is only slightly dependent on temperature, the activity of anorthite depends heavily on temperature for the observed plagioclase compositions in stage 2a (An40). As a result, the equilibria involving plagioclase becomes more dependent on temperature in particular for reaction (12). It can also

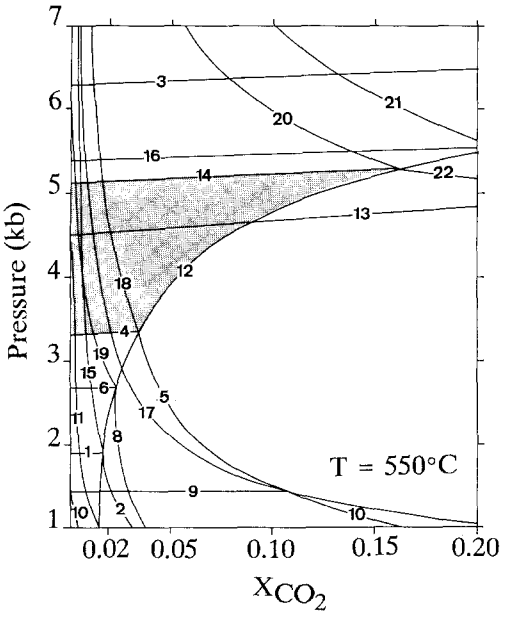

Fig. 3. Pressure-X_{CO_2} section for the system Si-Al-Ca-K-Ti-O-H-C for a temperature of 550 °C. The different equilibria (see listing in Table 3) were calculated for the following activity values of mineral end-members: anorthite = 0.86; muscovite = 0.75; titanite = 0.9; zoisite = 0.7; grossular = 0.85. Conditions of stage 1 of crystallization are given by the *shaded area*

Table 3. List of the reactions considered in Figs. 3 and 4

1: Kfs + 6 Zo = Ms + 2Gr + 6An + $2H_2O$
2: Kfs + 3Cc + 3An + H_2O = 2Gr + Ms + $3CO_2$
3: Mrg + 2aQz + 2Zo = 5An + $2H_2O$
4: aQz + 4Zo = Gr + 5An + $2H_2O$
5: aQz + 2Cc + An = Gr + $2CO_2$
6: 2Zo + 2Rt = An + Mrg + 2Tit
7: Cc + Mrg + 4Tit = 4Rt + 2Gr + H_2O + CO_2
8: 2Rt + Cc + 2An + H_2O = Mrg + 2Tit + CO_2
9: aQz + Gr = An + 2Wo
10: Gr + CO_2 = Wo + Cc + An
11: 5Cc + 8Zo = 3Mrg + 6Gr + H_2O + $5CO_2$
12: 2Zo + CO_2 = Cc + 3An + H_2O
13: Ms + aQz + Tit = Rt + Kfs + An + H_2O
14: 2Zo + 2aQz + Ms = 4An + Kfs + $2H_2O$
15: 2Cc + Kfs + 2Zo = Ms + 2Gr + $2CO_2$
16: aQz + Rt + 2Zo = Tit + 3An + H_2O
17: aQz + Cc = Wo + CO_2
18: 5Cc + 3aQz + 2Zo = 3Gr + H_2O + $5CO_2$
19: 6Tit + 3Mrg + CO_2 = Cc + 6Rt + 4Zo + H_2O
20: 4Cc + 3Ms + 6aQz = 2Zo + 3Kfs + $2H_2O$ + $4CO_2$
21: Rt + aQz + Cc = Tit + CO_2
22: Cc + Ms + 2aQz = Kfs + An + H_2O + CO_2
23: 4Zo + 3aQz = 5An + Gr + $2H_2O$
24: 2Zo + 3aQz + 5Cc = 3Gr + $5CO_2$ + H_2O
25: 5Cc + 3Mrg + 6aQz = 4Zo + H_2O + $5CO_2$

Assemblages on the left are stable on the high side of the Y-axis variable, or the high side of the X-axis variable for vertical reactions. Abbreviations: An = Anorthite, Cc = calcite, Zo = Zoisite, Mrg = margarite, Wo = wollastonite, Kfs = K feldspar, aQz = quartz α, Rt = rutile, Tit = titanite, Ms = muscovite, Gr = grossular

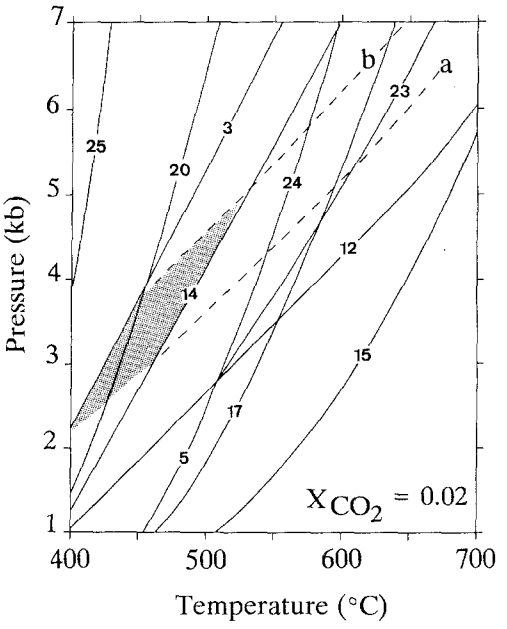

Fig. 4. Pressure-temperature section for the system Si-Al-Ca-K-O-H-C for $X_{CO_2} = 0.02$ and for the following activity values of mineral end-members: muscovite = 0.75; zoisite = 0.7; grossular = 0.85; anorthite = 0.93 at 400 °C to 0.58 at 700 °C. Equilibria are given in Table 3. Curves *a* and *b* represent equilibrium (12) for $X_{CO_2} = 0.03$ and $X_{CO_2} = 0.05$, respectively. Conditions of stage 2a of crystallization are given by the *shaded area*

be seen in Fig. 4 that the position of this equilibrium is highly dependent on X_{CO_2}. Indeed, for zoisite to remain stable during a slightly retrograded metamorphism (P decreasing from 4.5 to 4 kb, for example) X_{CO_2} cannot exceed 0.03 [curve (a) in Fig. 4]. The sericitization of feldspar according to reaction (14) is the result of a decrease of both temperature and pressure compared to stage 1. As margarite [curve (3), Fig. 4 and Table 3] has not been observed in the CSG, the P-T-X conditions of stage 2a are given by the grey area on Fig. 4; pressures ranging from about 3 to 4 kb and temperature from approx. 450 to 500 °C. Note that these low-to medium-pressure conditions are compatible with a high aluminium content in titanite (Gibert et al. 1990).

Stage 2b is characterized by the crystallization of idocrase and grossular. It can be seen in Fig. 4 that the formation of grossular [curves (24) and (5), Table 3] results from an increase of temperature. According to the experimental work of Hochella et al. (1982) idocrase crystallization requires a very low X_{CO_2}, and its association with quartz indicates probably a maximum temperature of about 500 °C for Fe-bearing idocrase. Thus, from a similar P-T plot calculated for $X_{CO_2} = 0.01$ the P-T conditions of stage 2b can be estimated to be about 2 kb and 500 °C.

Fluid compositions

A systematic study of fluid inclusions has yet to be performed on the scheelite deposits of the Schistes X series of the Montagne Noire. However, the regional metamorphic fluids from the Dôme de l'Agout (Axial Zone) and from the Schistes X series are known for their high gas content, including a relatively high proportion of nitrogen (Kreulen and Schuiling 1982; Bahdi and Moine 1992). For example, quartz-andalusite segregations related to the D2 event in the micaschists surrounding the CSG exhibit a majority of fluid inclusions composed only of CH_4 and N_2. Kreulen and Schuiling (1982) proposed a deep-seated source for N_2, while Duit et al. (1986) suggested that the breakdown of NH_4^+ -bearing micas was the main process producing the observed nitrogen. In a neighbouring region (Dôme de Montredon), a systematic determination of fluid inclusions compositions and of ammonium concentrations in micas and whole-rocks of the lower Cambrian series was performed by Guillot (1989). He showed that the dominant metamorphic fluids are aqueous solutions (about 90 mol %) of relatively low salinity (ca. 1 m NaCl) and a gaseous phase. N_2 (up to 25 mol % of the gas) was observed only in the black schists series, which also exhibits relatively high concentrations of ammonium. This suggests that the N_2 found in these fluid inclusions originated from primary organic compounds and the interaction between fluids and NH_4^+-bearing micas (Guillot et al. 1988; Guillot and Moine 1989). Note that the gas phase found in similar fluid inclusions in the scheelite bearing calc-silicate schists of the Dôme de Montredon is composed mainly of CH_4 and N_2. In general, the regional characteristics of the metamorphic fluids are compatible with the mineral associations described previously, suggesting low values of X_{CO_2} in the fluid phase of the CSG. In addition, it can be inferred that high concentrations of N_2 and CH_4 should have been present in the fluid, especially at stage 2 of metamorphism (Bahdi and Moine 1992). In conclusion, it can be deduced from petrological and mineralogical studies that tungsten was transported within the micaschists and deposited as scheelite only in the CSG of the Schistes X series at low-pressure.

To test whether these conditions are favourable for the transport of dissolved tungsten through aluminous rocks (i.e. micaschists) and its deposition as scheelite in the CSG, three major problems were examined: (1) the speciation of tungsten at about 500 °C and 2–4 kb in H_2O-NaCl solutions; (2) the solubility of scheelite in the CSG and in the micaschists; and (3) because of the presence of volatiles (specially N_2) in the thermal dôme of the Montagne Noire, the effect of N_2 on tungsten speciation and scheelite solubility. Similar processes are likely to operate for Sn transport and deposition in the Sn-bearing calc-silicates of stage 2a. However, it is not yet possible to model these processes because of the lack of thermodynamic data on the Sn end-members.

Speciation of tungsten in H_2O-NaCl solutions at high pressure and temperature

The aqueous chemistry of tungsten is simplified by the fact that only $W^{(VI)}$ is stable in most hydrothermal fluids. $W^{(V)}$ can become important at very low oxygen fugacity which is not likely to be encountered, even in the presence of graphite (Wood and Vlassopoulos 1989). The identification of the stable hydrolysis products of W^{6+} is difficult, as a result of slow reactions in solution, interference from transient and permanent precipitation, and because some of the stable species with fairly large polymeric ions (W_6 or W_{12}) are difficult to characterize. However, in hydrothermal solutions the situation is much simpler since polytungstates dominate the speciation of tungsten only at low temperature in acidic, W-enriched solutions (Wesolowski et al. 1984). It is generally agreed that at hydrothermal conditions the monomeric species are dominant: WO_4^{2-} in alkaline solutions, HWO_4^- and $H_2WO_4^0$ in neutral and acidic solutions. Several authors have suggested the formation of Na-W complexes in concentrated NaCl solutions. In particular, Wood and Vlassopoulos (1989) have pointed out that $NaHWO_4^0$ or $KHWO_4^0$ are probably the dominant species in concentrated solutions of NaOH, NaCl or KCl. Although Bryzgalin (1986) has called for the formation of WO_3Cl^- in supercritical NaCl and KCl solutions, it is unlikely that W-Cl complexes would be dominant since, even at very low pH, positively charged tungsten species do not form. This has been recently confirmed by the measurement of crystalline WO_3 solubility in concentrated solutions of HCl (up to 5 m) at 500 °C and 1 kb (Wood and Vlassopoulos 1989).

Assuming that, under metamorphic conditions, the W dominant species in hydrothermal fluids are WO_4^{2-}, HWO_4^-, $H_2WO_4^0$ and $NaHWO_4^0$, the following reactions, need to be considered to determine tungsten speciation:

$$H_2WO_4^0 = HWO_4^- + H^+ \quad (26)$$

$$HWO_4^- = WO_4^{2-} + H^+ \quad (27)$$

$$NaHWO_4^0 = HWO_4^- + Na^+ \quad (28)$$

Unfortunately no thermodynamic data on these reactions is currently available in the literature at temperatures above 300 °C.

Wesolowski et al. (1984) determined the equilibrium constant of reaction (27), K_{27}, to 300 °C under vapour pressure from potentiometric titrations in the system Na-WO_4-Cl-H_2O. At 300 °C they proposed that $\log K_{27} = -6.89$. These authors also measured the apparent dissociation constants Q of reactions (27) and (26 + 27) ($H_2WO_4^0 = WO_4^{2-} + 2H^+$) at 290 °C in 5.12 m NaCl aqueous solutions: $\log Q_{27} = -4.46$ and $\log Q_{(26+27)} = -7.27$ (where Q is expressed in molality units). From these data it follows that $\log Q_{26} = -2.81$. These data were used to deduce a value of K_{26} using the HKF model for activity coefficients in NaCl solutions (Helgeson et al. 1981). The activity coefficients for HWO_4^- and H^+ were approximated to be equal to those of Na^+. This calculation led to a value of $\log K_{26} = -4.3$ at 300 °C. To extrapolate the value of K_{26} and K_{27} to the conditions of precipitation of scheelite in the CSG (up to 550 °C and 4.5 kb) we have followed the approach of Franck (1956), Marshall and Franck (1981) and Anderson et al. (1991), which found linear relationships between the value of $\log K$ for most ion association reactions and the logarithm of the density of H_2O. The extrapolations were carried out by assuming the P-T dependences of $K(H_2WO_4)$ and $K(HWO_4^-)$ are similar to those of $K(H_2SO_4)$ (Quist et al. 1965) and $K(CaCl^+)$ (Frantz and Marshall 1982), respectively. The resulting $\log(K)$ values are reported in Table 4.

Table 4. Dissociation constants and solubility constants ($\log K$) used in the calculations

	300 °C Psat	1 kb	500 °C 2 kb	4 kb	
(26) $H_2WO_4^0 = HWO_4^- + H^+$	−4.3	−5.5	−4.2	−3.42	1
(27) $HWO_4^- = WO_4^{2-} + H^+$	−6.9	−8.1	−6.32	−5.1	1
(28) $NaHWO_4^0 = Na^+ + HWO_4^-$		0.48	1.28	1.59	2
(29) $WO_{3(c)} + NaOH^0 = NaHWO_4^0$		1.0			3
(30) $WO_{3(c)} + H_2O = H_2WO_4^0$		−2.55			3
(31) $H_2O = H^+ + OH^-$		−11.79	−10.23	−9.15	4
(32) $HCl^0 = H^+ + Cl^-$		−3.63	−2.32	−1.73	5
(33) $NaCl^0 = Na^+ + Cl^-$		−2.09	−1.06	−0.36	6
(34) $Na_2Cl^+ = NaCl^0 + Na^+$		−0.04	0.42	0.84	7
(35) $NaCl_2^- = NaCl^0 + Cl^-$		−0.04	0.42	0.84	7
(36) $Na_2Cl_2^0 = 2Na^+ + 2Cl^-$		−3.47	−1.80	−1.28	8
(37) $NaOH^0 = Na^+ + OH^-$		−3.16	−2.25	−1.9	9
(38) $KCl^0 = K^+ + Cl^-$		−3.13	−1.54	−0.82	10
(39) $KOH^0 = K^+ + OH^-$		−2.26	−1.68	−1.33	10
(40) $CaCl_2^0 = CaCl^+ + Cl^-$		−2.75	−1.64	−0.89	11
(41) $CaCl^+ = Ca^{2+} + Cl^-$		−5.31	−3.53	−2.32	11
(42) $CaWO_{4(c)} = Ca^{2+} + WO_4^{2-}$		−16.28	−11.95	−9.88	12

1 Data at 300 °C and Psat are from Wesolowski et al. (1984); other data are extrapolated (see text). 2 Calculated from Wood and Vlassopoulos (1989) at 1 kb, and extrapolated for higher pressure (see text). 3 Wood and Vlassopoulos (1989). 4 Marshall and Franck (1981). 5 Sverjensky et al. (1991). 6 Quist and Marshall (1968). 7 Oelkers and Helgeson (1990). 8 Oelkers and Helgeson (1992). 9 Extrapolated from Woodland and Walther data (1987). 10 Franck (1956). 11 Frantz and Marshall (1981). 12 Calculated using Helgeson et al. (1981), Jackson and Helgeson (1985) and Brown and Essene (1985) (see text)

Wood and Vlassopoulos (1989) deduced that $NaHWO_4^0$ is the dominant species in concentrated solutions of NaCl from solubility measurements of $WO_{3(c)}$ performed in alkaline solutions at 500 °C and 1 kb. Assuming that $NaHWO_4^0$ was the only significant tungsten species present in these experiments, Wood and Vlassopoulos (1989) calculated a value of $\log K_{29} = 1.0$ at 500 °C and 1 kb for the reaction:

$$WO_{3(c)} + NaOH^0 = NaHWO_4^0. \quad (29)$$

In addition, Wood and Vlassopoulos (1989) have derived a value of $\log K_{30} = -2.55$ for the reaction:

$$WO_{3(c)} + H_2O = H_2WO_4^0, \quad (30)$$

from the solubility measurements of $WO_{3(c)}$ carried out at 500 °C in HCl solutions where $H_2WO_4^0$ is the dominant species. Combining reactions (26), (29), (30) and the dissociation reactions of water (31) and of NaOH° (37) yields a value of $\log K_{28} = 0.48$ for the dissociation of $NaHWO_4^0$ at 500 °C and 1 kb [note that for this calculation a value of $\log K_{37} = -2.31$ was taken from Wood and Vlassopoulos (1989) who assumed K_{37} to be equal to the dissociation constant of $-K$ (KOH°), K_{38} in Table 4]. The value of $\log K_{28}$ at higher pressure was estimated using the "density" approach and assuming the pressure dependence of $K(NaHWO_4^0)$ to be similar to that of $K(KHSO_4^0)$, as determined by Quist and Marshall (1966).

To calculate the distribution of tungsten species as a function of pH in NaCl solutions were considered: H^+, OH^-, Cl^-, HCl^0, Na^+, $NaCl^0$, $NaOH^0$, WO_4^{2-}, HWO_4^-, $H_2WO_4^0$ and $NaHWO_4^0$. Thus, eleven equations are required to be solved for determining the solute speciation in this system. These equations include the law of mass action for the seven corresponding dissociation reactions listed in Table 4, charge balance constraints, and mass balance equations for sodium and tungsten. The pH in this system is varied by modifying Cl concentration. Activity coefficients of dissolved species were calculated after Helgeson et al. (1981), assuming $\gamma_i^{2+} = \gamma_i^{2-} = \gamma_{Ca}^{2+}$ and $\gamma_i^+ = \gamma_i^- = \gamma_{Na}^+$. The solution composition was calculated using a Newton-Raphson algorithm, the consistency between activity coefficients and the true ionic strength being obtained through an iterative method.

The distribution of W species as a function of pH is given in Fig. 5 at T = 500 °C and P = 2 and 4 kb in a 1 m NaCl aqueous solution, for W total = 10^{-3}m. It can be seen in Fig. 5 that the dominant solute species are WO_4^{2-} at 4 kb and WO_4^{2-}, HWO_4^- and $H_2WO_4^0$ at 2 kb. As a general rule WO_4^{2-} dominates in alkaline and neutral solutions while HWO_4^- and $H_2WO_4^0$ are important only in acidic solutions, particularly for the lower pressures. For pH ≤ 3 at 2 kb, the solution is dominated by $H_2WO_4^0$. Additional calculations were carried out taking into account the formation of the multi-ion clusters Na_2Cl^+, $NaCl_2^-$ and $Na_2Cl_2^0$ proposed by Oelkers and Helgeson (1990, 1992). In 1 m NaCl solutions it was found that the consideration of these clusters had a negligible effect on W speciation. It was found that the resulting change in solution pH and ionic strength are very small (i.e. at 500 °C and 1 kb for Na = Cl = 1 m, the calculated pH shifted only from 5.12 to 5.06 upon consideration of Na_2Cl^+, $NaCl_2^-$ and $Na_2Cl_2^0$).

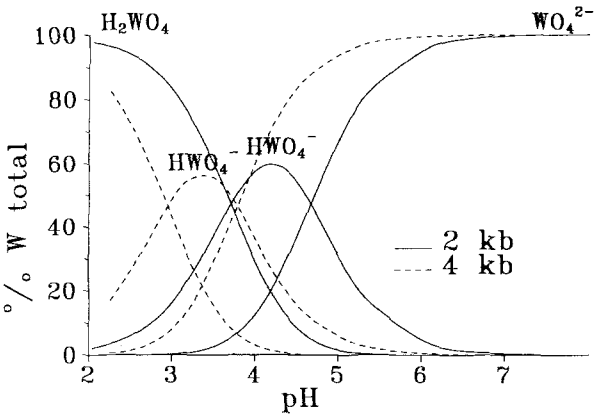

Fig. 5. Speciation of tungsten as a function of pH in NaCl (1 m) aqueous solutions for $\Sigma W = 10^{-3}$ m, T = 500 °C and P = 2 kb (*solid lines*) and 4 kb (*dashed lines*)

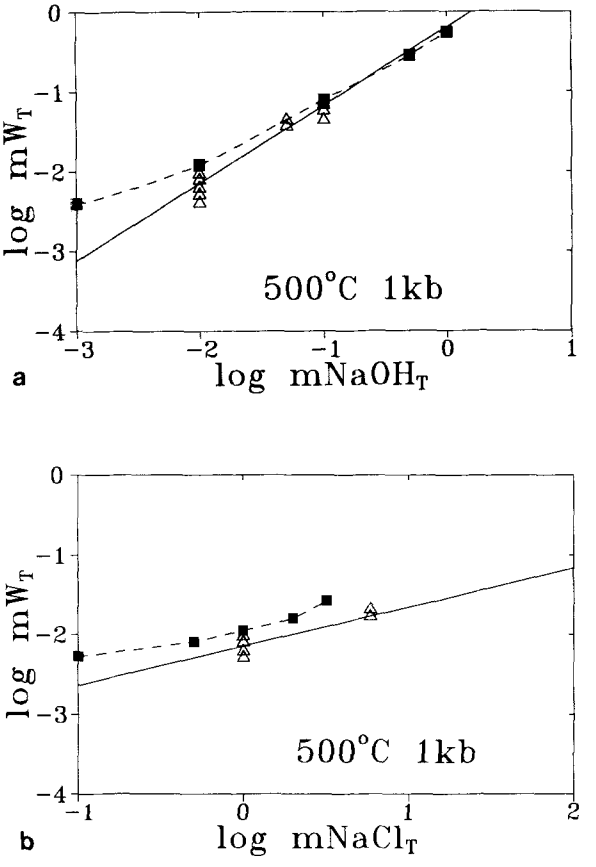

Fig. 6a, b. Solubility of crystalline WO_3 at 500 °C and 1 kb in aqueous solutions of **a** NaOH and **b** NaCl. *Triangles* and *solid lines* represent the experimental data of Wood and Vlassopoulos (1989). *Squares and dashed lines* represent the results of our calculations

The distribution of $NaHWO_4^0$ was not plotted in Fig. 5 because its concentration is extremely low (always less than 1% of total W), which contradicts the conclusion of Wood and Vlassopoulos (1989). Furthermore, the total concentration of dissolved tungsten in equilibrium with crystalline WO_3 was calculated as a function of NaOH concentration, ignoring $NaHWO_4^0$ and using the value of $\log K_{30}$ determined by Wood and Vlassopoulos (1989) for the dissolution of $WO_{3(c)}$ and the values of the association

constants for $H_2WO_4^0$, HWO_4^- and WO_4^{2-} given in Table 4. The good agreement observed between the calculated and measured W concentrations (Fig. 6a) demonstrates that there is no need to consider $NaHWO_4^0$ to reproduce the solubility data. A similar calculation carried out for $WO_{3(c)}$ solubility in H_2O-NaCl solutions leads to the same conclusion (Fig. 6b). The important role ascribed by Wood and Vlassopoulos (1989) to $NaHWO_4^0$ results from the fact that they assumed that $H_2WO_4^0$ was the dominant species for the whole range of pH and that they ignored the formation of negative charged species in neutral and alkaline solutions. As a result, they explained the increase of $WO_{3(c)}$ solubility as a function of NaOH concentration through the formation of the $NaHWO_4^0$ complex rather than due to an increase of pH favouring the formation of WO_4^{2-}, along with the decrease of the activity coefficients as a function of the ionic strength. The formation in alkaline solutions of complexes involving Na^+ and WO_4^{2-} (i.e. $NaHWO_4^0$, $NaWO_4^-$ or $Na_2WO_4^0$) cannot be totally ruled out, however this assumption cannot be further investigated from the Wood and Vlassopoulos (1989) data, because, for a given NaOH concentration, they did not perform experiments as a function of NaCl concentration, which is the only way to separate the effect of pH from those due to the possible formation of Na-W complexes. In conclusion it appears that WO_4^{2-}, HWO_4^- and $H_2WO_4^0$ are the dominant W-bearing aqueous species at 500 °C and 2 and 4 kb.

Scheelite solubility

Role of presssure and host mineral assemblage

In a solution in chemical equilibrium with the micaschists or the CSG assemblage and scheelite the following major aqueous species, besides W species, should be taken into account: Na^+, $NaOH^0$, $NaCl^0$, K^+, KOH^0, KCl^0, Ca^{2+}, $CaCl^-$, $CaCl_2^0$, HCl^0, H^+, OH^- and Cl^-. At a given temperature, pressure and Cl molality, the composition of the solution is constrained by the mineral assemblage which determines the values of the activity ratios $a_{Ca^{2+}}/a_{H^+}^2$, a_{Na^+}/a_{H^+}, a_{K^+}/a_{H^+}.

These ratios can be determined using activity-activity diagrams calculated with true mineral compositions. For example, Fig. 7 shows a $\log(a_{K^+}/a_{H^+})$ versus $\log(a_{Ca^{2+}}/a_{H^+}^2)$ plot for minerals corresponding to the stage 1 paragenesis at 550 °C and 4.5 kb. It can be seen here that the association Czo(Ps10) + K-Feldspar + An90 constraints the values of $a_{Ca^{2+}}/a_{H^+}^2$ and a_{K^+}/a_{H^+}. Then the value of a_{Na^+}/a_{H^+} can be calculated from the plagioclase composition. Thermodynamic data used for calculation of scheelite dissolution constant (K_{42} in Table 4) were taken from Brown and Essene (1985) for $CaWO_4$, Jackson and Helgeson (1985) for WO_4^{2-} and Helgeson et al. (1981) for Ca^{2+}. The fluid compositions in equilibrium with the micaschists and the CSG were calculated taking into account the activity ratios and the scheelite dissolution constant. The results of these calculations are given in Table 5 for stage 1 and stage 2b.

As emphasized already, temperature exerts an important control on scheelite solubility. For example, in the P-T range of interest (450–550 °C and 2–4.5 kb) its solubility decreases by approximately one order of magnitude as the temperature is lowered 100 °C at constant pressure, chlorinity and rock composition. However, the most striking characteristic of scheelite deposition in the Montagne Noire is that it occurred at a relatively low-pressure. Figure 8 illustrates scheelite solubility as a function of

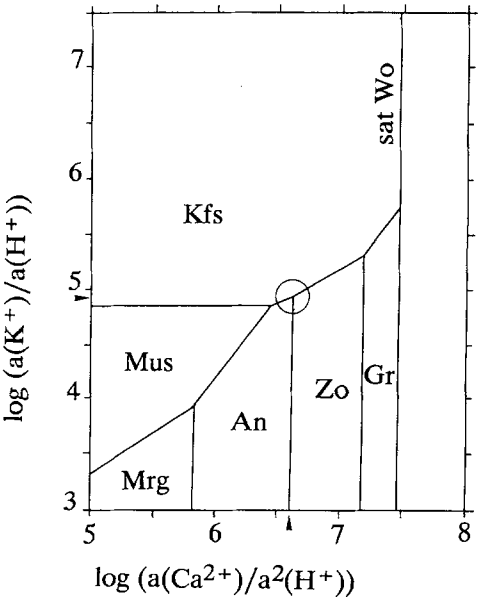

Fig. 7. Plot of $\log(a_{K^+}/a_{H^+})$ as a function of $\log(a_{Ca^{2+}}/a^2_{H^+})$ for the mineral assemblage of stage 1 CSG (T = 550 °C, P = 4.5 kb and $X_{CO_2} = 0.1$). See Table 3 for the significance of the abbreviations

Table 5. Calculated compositions (molalities) of the aqueous solutions in equilibrium with the micaschists and CSG assemblages of stages 1 and 2b, respectively

	Stage 1		Stage 2b	
	Micaschists	CSG	Micaschists	CSG
aCa^{2+}/a^2H^+	5.95	6.65	5.48	7.05
aK^+/aH^+	4.85	5.11	4.61	4.83
aNa^+/aH^+	5.20	5.06	4.90	4.96
OH^-	1.73 E-03	2.01 E-03	1.27 E-04	1.76 E-04
H^+	2.67 E-06	2.27 E-06	4.00 E-06	2.79 E-06
Cl^-	5.84 E-01	5.43 E-01	4.80 E-01	4.29 E-01
HCl^0	3.77 E-05	3.03 E-05	4.63 E-05	3.01 E-05
Na^+	4.23 E-01	2.26 E-01	3.18 E-01	2.54 E-01
$NaCl^0$	1.76 E-01	1.03 E-01	2.02 E-01	1.51 E-01
$NaOH^0$	1.58 E-02	1.15 E-02	8.32 E-04	9.55 E-05
K^+	1.89 E-01	2.29 E-01	1.63 E-01	1.89 E-01
KCl^0	2.38 E-01	3.48 E-01	3.13 E-01	3.37 E-01
KOH^0	1.99 E-03	3.63 E-03	1.15 E-04	1.91 E-04
Ca^{2+}	6.94 E-04	2.19 E-04	5.74 E-05	9.58 E-04
$CaCl^+$	3.64 E-04	1.25 E-03	9.08 E-04	1.53 E-02
$CaCl_2^0$	6.50 E-04	2.11 E-03	2.14 E-03	3.36 E-02
WO_4^{2-}	1.31 E-02	3.05 E-03	2.06 E-04	9.77 E-06
HWO_4^-	1.95 E-04	4.50 E-05	1.68 E-05	6.23 E-07
$H_2WO_4^0$	2.63 E-07	5.25 E-08	1.23 E-07	3.31 E-09
$NaHWO_4^0$	5.75 E-08	8.32 E-09	3.24 E-08	1.00 E-10
W_{total} (ppm)	2440	570	41.06	1.91

pressure for two mineral assemblages typical of the micaschists (Qz, Kfs, Ms, An15) and CSG of stage 1 [Qz, Czo (Ps10), An90, Kfs] [note that below 3 kb the association of An90 and Czo (Ps10) is no longer stable and that clinozoisite is replaced by grossular]. It can be seen in Fig. 8 that decreasing pressure strongly favours scheelite precipitation and that solutions equilibrated with the micaschists (curve A) accommodate higher W concentrations than those in equilibrium with the calc-silicate gneisses (curve B). Note also that the ratio (R) between these two concentrations at a given pressure, is relatively low and remains constant ($R = 4$) when pressure varies.

Scheelite solubility is further decreased when the mineralogical variations occurring in the CSG between stage 1 and 2 (see Table 1) are taken into account (Fig. 9; compare Figs. 8 and 9). Furthermore, the ratio (R) increases from $R = 4$ for stage 1 paragenesis to about 20 in the case of the CSG of stage 2b, where scheelite precipitation was observed. Thus, a major reason why scheelite deposition is restricted to the CSG are the mineralogical changes that occur at stage 2b.

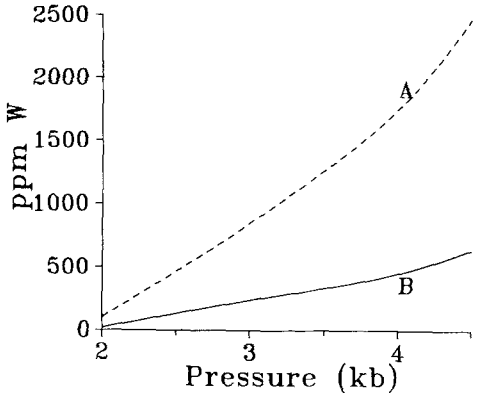

Fig. 8. Variation of scheelite solubility as a function of pressure at 550 °C in solutions in equilibrium with the mineral assemblages. *Dashed line* (A) = micaschists (Qz, Kfs, Ms, An15) and *solid line* (B) = stage 1 CSG (Qz, Czo (Ps10), Kfs). R (in the text) denotes the ratio between W concentration along (A) and (B) at a given pressure

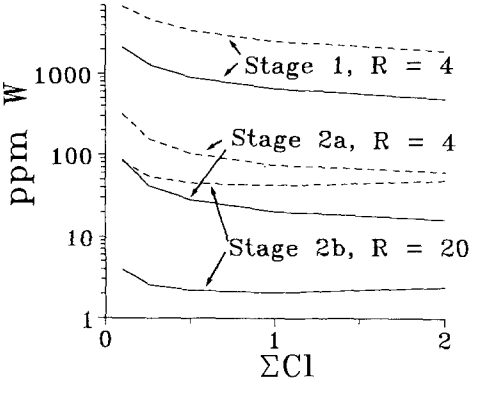

Fig. 9. Variations of scheelite solubility in solutions in equilibrium with the micaschists (*dashed lines*) and with CSG (*solid lines*) in the course of metamorphism and alteration from stage 1 (550 °C; 4.5 kb) to stage 2a (450 °C; 3 kb) and stage 2b (500 °C; 2 kb). R has the same definition as in Fig. 8

Figure 9 also shows that aqueous tungsten concentration decreases with increasing chlorinity. Note this trend is opposite to that observed in experimental dissolution of scheelite in H_2O-NaCl solution. By contrast with scheelite dissolution experiments in the laboratory, under natural conditions the concentration of Ca in solution is controlled by heterogeneous equilibrium with silicate minerals and increases with increasing Cl molality. Thus, an increase in aqueous Cl concentration in natural systems results in a decrease of W concentration.

Speciation of tungsten and scheelite solubility in H_2O–NaCl–N_2 mixtures

In general, the addition of nonpolar volatiles like N_2, CH_4, and CO_2 results in a dramatic decrease of the dielectric constant (ε) of the solution at a given pressure and temperature. For example, it can be seen in Fig. 10, where the dielectric constant of H_2O-N_2 mixtures is plotted at 500 °C and 2 and 4 kb, that the addition of 15 mol % of N_2 to water reduces the value of ε to one half of its value. In accord with Coulomb's law and the Born equation, this reduction in ε changes the interactions among dissolved species and between the solvent and aqueous species.

Assuming that the solvent is a dielectric continuum, the excess Gibbs free energy of dissolved species in crustal fluids ($\Delta G^*_{ex,i}$) can be predicted from (Schott and Dandurand 1987; Walther and Schott 1988; Dandurand and Schott 1987, 1992):

$$\Delta G^*_{ex,i} = \Delta G^*_{DH,i} + \Delta G^*_{sr,i} + \Delta G^*_{solv,i} \quad (43)$$

where $\Delta G^*_{DH,i}$ accounts for long-range ionic interactions (Debye-Hückel term), and $\Delta G^*_{sr,i}$ for short-range interactions between ions and dipoles of different types (Brönsted term). $\Delta G^*_{solv,i}$ is a solvation term which accounts for the free energy change associated with removing an ion from water and placing it in a different solution (for

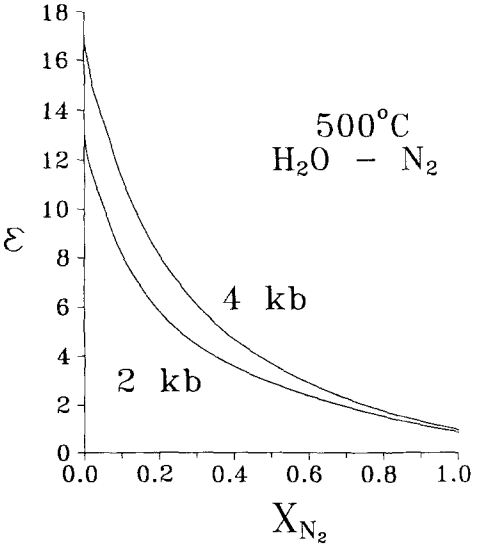

Fig. 10. Calculated dielectric constant of H_2O-N_2 mixtures at 500 °C and 2 kb and 4 kb, respectively

example a mixture of water with a nonpolar volatile like N_2). $\Delta G^*_{solv,i}$ can be expressed by the classical Born (1920) equation:

$$\Delta G^*_{solv,i} = N^\circ Z_i^2 e^2 (1/\varepsilon - 1/\varepsilon_w)/2r_i \quad (44)$$

where N^0 is the Avogadro number, e the electronic charge, Z_i the ionic charge, r_i is the radius of the ion and ε and ε_w are the dielectric constants of the solvent mixture and H_2O, respectively. It follows from Eq. (43) and the definition of the activity coefficient ($\ln \gamma_i = \Delta G^*_{ex,i}/RT$) that:

$$\gamma_i = \gamma_{DH,i} \cdot \gamma_{sr,i} \cdot \gamma_{solv,i} \quad (45)$$

The analysis of experimental mineral solubility data with Eqs. (43) and (45) indicates that $\gamma_{solv,i}$ is by far the most important contribution to γ_i in solutions containing substantial amounts of volatiles or organic compounds (Dandurand and Schott 1992; Fein and Walther 1989). Thus, solvent-ion or solvent-dipole interactions are likely to dominate in crustal fluids containing nonpolar volatiles.

The striking simplicity of the Born model has led to its widespread application for prediction of ion/dipole-solvent interactions. However, two objections are frequently raised against the Born treatment of solvation. One objection concerns the use of the macroscopic quantity ε (this treatment is particularly questionable in describing the immediate vicinity of an ion in solution where strongly inhomogeneous fields up to 10^8 V/m exist). The second concerns the interpretation of the Born radius r_i. A detailed discussion of these limitations is beyond the scope of this paper (i.e. see Bucher and Porter 1986 or Dandurand and Schott 1992 for a thorough discussion of these objections). These limitations have been overcome by using the "dual solvent region model" developed by Abraham and Liszi (1978), and Dandurand and Schott (1992) to calculate $G^*_{solv,i}$. In this model an ion (or a dipole) of radius r_i is surrounded by an organized solvent layer of thickness $(b - r_i)$ with a dielectric constant ε_1; beyond this layer exists the bulk solvent, assumed to be a dielectric continuum. The thickness of the solvent organized layer for most monovalent cations is estimated to be equal to the radius of the water molecule ($r_{H_2O} = 1.5$ Å). Bivalent cations are assumed to be surrounded by two layers of organized water ($b - r_i = 2r_{H_2O}$); also it is assumed that these cations retain one water layer when they form complex ions or neutral species by contact with anions. In agreement with Latimer et al. (1939), it was assumed that monovalent anions are not surrounded by an organized solvent layer ($b - r_i = 0$). Within this framework, the free energy of solvation of an ion i, $G^*_{solv,i}$ can be expressed as (Dandurand and Schott 1992):

$$G^*_{solv,i} = N^0 Z^2 e^2 ((1/\varepsilon_1 - 1)/r_i - (1/\varepsilon_1 - 1/\varepsilon)/b)/2 \quad (46)$$

where r_i is the ionic crystal radius, ε is the dielectric constant of the bulk solvent mixture and $\varepsilon_1 = 2$.

This model was applied to predict the speciation of tungsten and the solubility of scheelite in H_2O-NaCl-N_2 solutions. The HKF model was used [Eq. (298), p. 1478 in Helgeson et al. 1981] to calculate the product $\gamma_{DH,i} \cdot \gamma_{sr,i}$. The solvation Gibbs free energy was deduced from Eq. (46). Values of γ_i for ions and dipoles used in these calculations are listed in Table 6. The dielectric constants of H_2O-NaCl (1 m)-N_2 mixtures were assumed to be equal to those of H_2O-N_2 mixtures because, at this concentration, NaCl has little effect on ε (Walther and Schott 1988). Following the approach of Looyenga (1965), the dielectric constant of mixtures of water with other volatiles was obtained using a truncated Taylor expansion for the volume of mixing and the dielectric constant of the end-members:

$$\varepsilon_m = [\varepsilon_v^{1/3} + \Phi_w(\varepsilon_w^{1/3} - \varepsilon_v^{1/3})] \quad (47)$$

where the subscripts v and w stand for the pure nonpolar volatile and H_2O respectively, and Φ is the volume fraction in the mixture. Φ_w in H_2O-N_2 mixtures was obtained from a modified Redlich-Kwong equation (Holloway 1977, 1981; Flowers 1979). The dielectric constants of pure H_2O and N_2 were calculated from the Kirkwood (1939) equation given by:

$$(2\varepsilon + 1)(\varepsilon - 1)/9\varepsilon = (4\pi N^0 \rho/3M)(\alpha + \mu^2 g/3kT) \quad (48)$$

where ρ and M are the density and molecular weight of the pure fluid, respectively; k is the Boltzmann constant and T is temperature in K; α and μ are the molecular polarizability and dipole moment, respectively and g, the "Kirkwood orientation factor", quantifies the local ordering between polar molecules in the fluid phase. Values of g for pure H_2O were obtained from equations and parameters reported by Pitzer (1983), whereas, because $\mu = 0$, a value of g is not necessary for the calculation of the dielectric constant of N_2. Values of α and μ were obtained from Böttcher et al. (1973). Densities of N_2 were computed using the Redlich-Kwong equation. Calculated ε values for H_2O-N_2 mixtures at 500 °C and 2 and 4 kb are shown in Fig. 10.

The addition of a nonpolar volatile like N_2 to ore-forming hydrothermal solutions has two main conse-

Table 6. Values of the contribution of solvation $\gamma_{solv,i}$ to the activity coefficient of ions and dipoles in H_2O-N_2 mixtures (T = 500°C, P = 2 kb)

	r_i(Å)	Number of H_2O layers	b (Å)	log γ_i 5% N_2	log γ_i 10% N_2
H^+	–	1	1.6[a]	0.63	1.36
Na^+	0.97	1	2.47	0.41	0.88
K^+	1.33	1	2.83	0.36	0.77
Ca^{2+}	0.99	2	3.99	1.02	2.18
Cl^-	1.81	0	1.81	0.56	1.20
OH^-	1.40[b]	0	1.40	0.73	1.55
WO_4^{2-}	1.89[c]	1[d]	3.39	1.20	2.57
HWO_4^-	2.30[c]	1	3.80	0.27	0.57
$CaCl^+$	–	1	4.30	0.23	0.51
$H_2WO_4^0$	–	0	2.30	0.07	0.15
$NaHWO_4^0$	–	0	3.28	0.05	0.11
$NaCl^0$	–	0	2.78	0.06	0.13
$NaOH^0$	–	0	2.37	0.07	0.15
KCl^0	–	0	3.12	0.05	0.11
KOH^0	–	0	2.73	0.06	0.13
$CaCl_2^0$	–	1	4.66	0.03	0.07
HCl^0	–	0	2.01	0.08	0.17

Crystal radii (r_i) are from Pauling unless noted otherwise.
[a] Approximated to the radius of H_2O; [b] from Shock and Helgeson (1988); [c] calculated in this study from the crystal radii of W^{6+} and O^{2-}; [d] the bivalent anion, WO_4^{2-}, was assumed to be surrounded by one layer of solvent

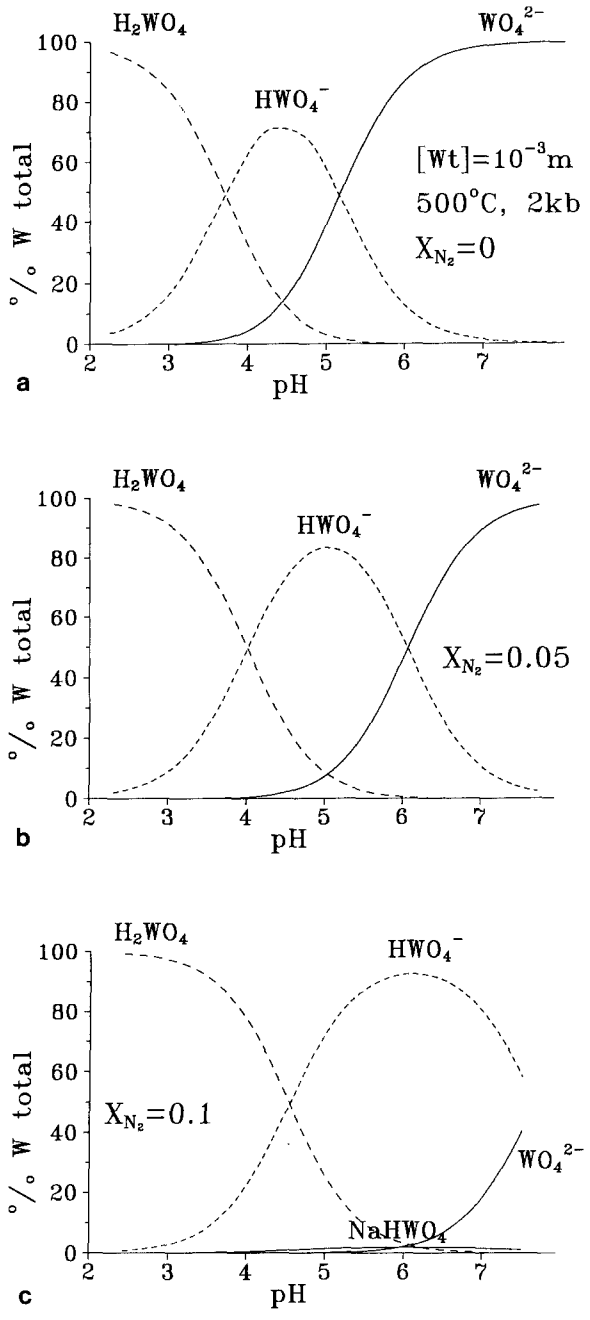

Fig. 11a–c. Calculated distribution of tungsten species as a function of pH in H_2O-N_2-NaCl (1 m) mixtures at 500 °C and 2 kb and for $\Sigma W = 10^{-3}$ m. **a** $X_{N_2} = 0$; **b** $X_{N_2} = 0.05$; **c** $X_{N_2} = 0.1$

quences: (1) a modification of the distribution of metal aqueous species as a result of changes of their apparent association constants and (2) a decrease of the solubility of minerals because of the increase of activity coefficients. The consequences of these factors can be seen in Fig. 11 which shows the computed distribution of tungsten among aqueous species as a function of pH at 500 °C and 2 kb for N_2 mole fractions ranging between 0 and 0.1. For a solution with a pH of approx. 4.5 to 6.5, the addition of N_2 results in a marked increase in $H_2WO_4^0$ and HWO_4^- concentrations relative to WO_4^{2-}. The relative decrease of WO_4^{2-} becomes more important at lower pHs and higher N_2 concentrations. One might expect the relative increase

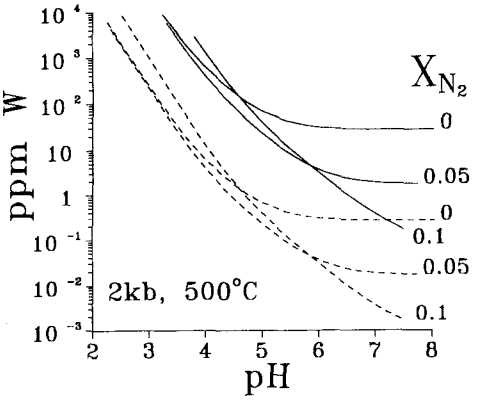

Fig. 12. Solubility of scheelite as a function of pH in H_2O-N_2-NaCl (1 M) mixtures at 500 °C, 2 kb and for $\log(a_{Ca^{2+}}) = -6$ (*solid lines*) and $\log(a_{Ca^{2+}}) = -4.5$ (*dashed lines*), respectively

of HWO_4^- and $H_2WO_4^0$ to favour W transport in hydrothermal solutions where mWO_4^{2-} is controlled by scheelite solubility. However, calculation of scheelite solubility for two likely values of $a_{Ca^{2+}}$ in equlibrium with micaschists ($\log a_{Ca^{2+}} = -6$) and calc-silicate rocks ($\log a_{Ca^{2+}} = -4.5$) indicates that this generally is not the case (Fig. 12), as the increase of WO_4^{2-} activity coefficient due to the addition of N_2 often dominates the effects of the changes in the distribution of W aqueous species. Thus, the addition of N_2 results in a significant decrease in scheelite solubility, favouring its precipitation. In addition, this effect is less significant in acidic conditions where the contribution of WO_4^{2-} to W-total becomes negligible. Furthermore, scheelite solubility does not change significantly when X_{N_2} increases from 0.05 to 0.1 at a pH of 5.5–6. Note that incorporation of triple and quadruple NaCl clusters has a negligible effect on tungsten distribution even at 10 mol % of N_2. This solubility decrease is of the same order of magnitude as the corresponding decrease in portlandite solubility with increasing Ar concentration in H_2O-Ar mixtures at 500 °C and 2 kb measured by Fein and Walter 1989 (for $X_{Ar} = 0.1$ they found a decrease of the molality of calcium by a factor of 5).

Conclusions

The observations and calculations summarized here leave little doubt that large amounts of tungsten (up to a few thousand ppm) can be accommodated by aqueous solutions circulating within a micaschist or a CSG environment at high P-T conditions (i.e. 550 °C and 4.5 kb). However, such concentrations are generally not observed because of the relatively low quantities of tungsten which are available in the source rocks. For example, the W-content of the micaschists in the Montagne Noire is about 3–4 ppm. This regional concentration probably corresponds to the original sedimentary concentration as established on the basis of numerous analyses of regional rocks at various metamorphic grades (Caleffi et al. 1988; Couilloud 1988; Guillot 1989; Gibert 1991). Assuming micas were the main tungsten-bearing minerals, their W-content should not exceed 50 ppm and one could expect a maximum concentration of about 10 ppm W in equilibrated

solutions. Mass balance considerations reveal that for a plausible water/rock ratio during the stage 2b event of 1000, such hydrothermal fluids would have precipitated 3 ppm W as scheelite in the CSG to obtain a concentration of 3000 ppm in the mineralized rocks (or 1 ppm W if the water/rock ratio = 3000). Thus the W-content of the mineralizing fluids was probably between a few ppm and 10 ppm. The petrological and mineralogical study indicates that these fluids were undersaturated with respect to scheelite in the micaschist environment but supersaturated in the CSG. It can be concluded from the results presented that pressures as low as 2000 bar at 500 °C are necessary for scheelite to precipitate only in the GSC (see Fig. 9). Under these conditions, a large solubility contrast (about 20) is obtained when the mineralizing solutions circulate from the micaschists to idocrase- and grossular-bearing CSG.

In addition, these results demonstrate that the addition of nonpolar volatiles like N_2 to the mineralizing solutions results in a strong decrease of scheelite solubility in the solution pH range consistent with common metamorphic assemblages (pH about 5.5–6). The presence of such volatiles, by extending the range of P, T and $a_{Ca^{2+}}$ allowing scheelite precipitation, is thus likely to favour its formation and this might explain the frequent association of W (and Sn) deposits with graphitic series generating mixed volatiles fluids. Such fluids were present in the CSG as well as in the micaschists in the Montagne Noire during scheelite deposition. In the CSG environment scheelite saturation is obtained for low W concentrations (about 2 ppm in aqueous solutions). Thus, the addition of volatiles is likely to enhance scheelite crystallization. As demonstrated by the field observations, scheelite saturation was never reached in the micaschist environment. It thus appears that large amounts of volatiles were not present in the mineralizing fluids. For example, the addition of only 5% of N_2 would decrease the solubility of scheelite in the micaschists from 40 ppm to less than 3 ppm W.

Ackowledgements. This is CNRS/INSU/DBT contribution number 440. Financial support was provided by the Institut National des Sciences de l'Univers (Thème "Fluides et Cinétique" of the Program "Dynamique et Bilan de la Terre" and ARC tungstène of the PIRSEM). Field work has benefited from discussions with Pierre Beziat, Serge Bogdanof, Michel Demange and Alain Ploquin. We thank Harold C. Helgeson, Marie-Lola Pascal and Vitalii Pokrovskii for providing beneficial reviews of the manuscript. An early version of the paper was improved by Linda Richard. Eric Oelkers was unlucky enough to be around at the stage where English editing of the manuscript was deeply needed: his desperate fight trying to fade bright occitano-gallic colours of this manuscript was very impressive. We are also grateful to Eric for helpful discussions and preprints of his work in advance of publication.

References

Abraham MH, Liszi J (1978) Calculation of ionic solvation. Part 1. Free energy of solvation of gaseous univalent ions using a one-layer continuum model. J Chem Soc, Faraday Trans 1.74:1604–1614

Anderson GM, Castet S, Schott J, Mesmer RE (1991) The density model for estimation of thermodynamic parameters of reactions at high temperature and pressure. Geochim Cosmochim Acta: 55:1769–1779

Arthaud F (1970) Etude tectonique et microtectonique comparée de deux domaines hercyniens: les nappes de la Montagne Noire (France) et l'anticlinorium de l'Iglesiente (Sardaigne). Unpub. PhD thesis, Montpellier University, France

Badhi M, Moine B (1992) Les fluides carbo-azotés du dôme de l'Agout (Montagne Noire). 14th Earth Sciences Meeting, Toulouse, April 1992, France

Berman RG (1988) Internal-consistent thermodynamic data for stoichiometric minerals in the system Na_2O-K_2O-CaO-MgO-FeO-Fe_2O_3-Al_2O_3-SiO_2-TiO_2-H_2O-CO_2. J Petrology 29:445-522

Berman RG, Brown TH, Perkins EH (1987) GEO-CALC: software for calculation and display of P-T-X phase diagrams. Am Mineral 72:861-862

Bird DK, Helgeson HC (1980) Chemical interaction of aqueous solutions with epidote-feldspar mineral assemblages in geologic systems. I. Thermodynamic analysis of phase relations in the system CaO-FeO-Fe_2O_3-Al_2O_3-SiO_2-H_2O-CO_2. Am J Sci 280:907-941

Bouchardon JL, Dechomets R, Demange M (1979) A propos du disthène en roche dans les micaschistes et les gneiss du synclinal de Rosis et du flanc sud, zone axiale de la Montagne Noire (Massif Central français). C.R. Acad. Sci., Paris D 259:4309–4312

Böttcher CJF, Van Belle OC, Bordewijk P, Rip A (1973) Theory of electric polarization. Elsevier, Amsterdam, Netherlands

Born Von M (1920) Volumen and hydratations wärme der ionen. Z Phys 1:45–48

Boyer F, Routhier P (1974) Extension régionale de couches à scheelite dans la couverture métamorphique de la zone axiale en Montagne Noire (Hérault, France). C.R. Acad. Sci. Paris, série D 279:1829–1832

Brown TH, Berman RG, Perkins EH (1989) PTA-SYSTEM: Geo-Calc software package for the calculation and display of activity-temperature-pressure phase diagrams. Am Mineral 74:485–487

Brown PE, Essene EJ (1985) Activity variations attending tungsten skarn formation, Pine Creek, California. Contrib Mineral Petrol 89:358–369

Bryzgalin (1986) In: Mineralogy and geochemistry of tungsten deposits. Leningrad, USSR pp 209–214 (in Russian)

Bucher M, Porter TL (1986) Analysis of the Born model for hydration of ions. J Phys Chem 90:3806–3411

Caleffi D, Moine B, Beziat P, Tollon F (1988) Etude géochimique et minéralogique de la "Série Noire" du Cambrien inférieur de la Montagne Noire. Origine des minéralisations stratiformes à scheelite de l'Hom-Haut (district de Montredon). In: Johan Z, Ohnenstetter D (eds) Gisements métallifères dans leur contexte géologique. Doc BRGM, Orléans, pp 158, 195–217

Cheilletz A (1983) Les lentilles rubanées stratiformes à scheelite-biotite de Djebel Aouam, Maroc central. Première description et interprétation. CR Acad Sci, Paris, 297, 581–584

Cheilletz A (1988) Stratiform tungsten deposits: a review. Geol Mijnbounw 67:293–311

Couilloud D (1988) Etude pétrographique, minéralogique et géochimique des skarns à tungstène de Fumade (Tarn, France). Unpubl. PhD, Toulouse University, France

Dandurand JL, Schott J (1987) New data on the solubility of amorphous silica in organic compound-water solutions and a new model for thermodynamic behavior of aqueous silica in aqueous complex solutions. J Solution Chem 16:237–256

Dandurand JL, Schott J (1992) Prediction of ion association in mixed crustal fluids. J Phys Chem (in press)

De Smedt, Sonnet P (1988) Genesis of scheelite-bearing calcsilicate gneisses in the Tanneron Massif (Var, France). In: Boissonnas J, Omenetto P (eds) Mineral deposits within the European Community. Springer, Berlin Heidelberg New York, pp 160–178

Demange M (1982) Etude géologique du massif de l'Agout, Montagne Noire, France. Unpub. thesis, Paris VI University, France

Demange M (1985) The eclogite-facies rocks of the Montagne Noire, France. Chem Geol 50:173–188

Demange M, Goutay R, Issard H, Perrin M (1986) Présence de disthène épizonal dans la zone axiale de la Montagne Noire (Massif Central, France). Bull Soc Géol Fr (8)2: 525–526

Derré C, Lecolle M, Roger G (1982) Les quartzites à silicates calciques et scheelite: préconcentrations familières ou pièges pour un tungstène étranger lié à l'hydrothermalisme périgranitique? Exemple du Nord-Est Transmontain (Portugal). Miner Deposita 17:363–385

Dubessy J, Ramboz C, Nguyen-Trung C, Cathelineau M, Charoy B, Cuney M, Leroy J, Poty B, Weisbrod A (1987) Physical and chemical controls (fO_2, T, pH) of the opposite behaviour of U and Sn-W as examplified by hydrothermal deposits in France and Great Britain, and solubility data. Bull Mineral 110:261–281

Duit W, Jansen JBH, van Breemen A, Bos A (1986) Ammonium micas in metamorphic rocks as examplified by Dôme de l'Agout (France). Am J Sci 286:702–732

Fein JB, Walther JV (1989) Portlandite solubilities in supercritical Ar-H_2O mixtures: implication for quantifying solvent effects. Am J Sci 289:975–983

Flowers GC (1979) Correction of Holloway's (1977) adaptation of the modified Redlich-Kwong equation of state for calculation of the fugacities of molecular species in supercritical fluids of geologic interest. Contrib Mineral Petrol 69:315–318

Fulp MS, Renshaw JL (1985) Volcanogenic-exhalative tungsten mineralization of Proterozoic age near Santa Fe, New Mexico, and implication for exploration. Geology 13:66–69

Franck EU (1956) Hochverdichteter Wasserdampf III. Ionendissoziation von KCl, KOH und H_2O in überkritischem Wasser. Z Phys Chem 8:192–206

Frantz JD, Marshall WL (1982) Electrical conductances and ionization constants of calcium chloride in aqueous solutions at temperatures to 600 °C and pressures to 4000 bars. Am J Sci 282:1666–1693

Gèze B (1949) Etude géologique de la Montagne Noire et des Cévennes méridionales. Mém Soc Geol Fr Nlle 29, 215 p

Gibert F (1991) Les gneiss à silicates calciques des Schistes X de la Montagne Noire. Origine et modalités de la metasomatose et du depot de W et Sn. Unpubl. PhD, Toulouse University, France

Gibert F, Caleffi D, Gibert P, Moine B (1989) Metamorphic processes in the formation of scheelite deposits within calc-silicate gneisses. Terra Abstract 1, 1, 121

Gibert F, Moine B, Beziat P (1988) Les gneiss à silicates calciques minéralisés en W-Sn dans la série des Schistes X, à la terminaison orientale de la Montagne Noire. Résultats priliminaires. In: Johan Z, Ohnenstetter D (eds) Gisements métallifères dans leur contexte géologique. Doc BRGM, 158, 219–244

Gibert F, Moine B, Gibert P (1990) Titanites (sphènes) alumineuses formées à basse/moyenne pression dans les gneiss à silicates calciques de la Montagne Noire. CR Acad Sci Paris, 311:657–663

Guillot C (1989) Origine et comportement de l'azote dans les formations métamorphiques: étude des inclusions fluides et géochimie de l'ammonium dans le Dôme de Montredon (Montagne Noire, France). Unpub. PhD, Toulouse University, France

Guillot C, Moine B (1989) Relationships between N_2 in the fluid inclusions and NH_4^+ in rocks (and micas) in the Dôme de Montredon, Montagne Noire, France. In: ECROFI X abst, London, p 41

Guillot C, Moine B, Beny C, Tollon F, Touray JC (1988) Repartition and origin of N_2 in the fluid inclusions of the Dôme de Montredon, Montagne Noire, France. Chem Geol 70:163

Helgeson HC, Kirkham DH, Flowers GC (1981) Theoretical prediction of the thermodynamic behavior of aqueous electrolytes at high pressures and tempeatures: IV. Calculation of activity coefficients, osmotic coefficients, and apparent molal and standard and relative partial molal properties to 600 °C and 5 kb. Am J Sci 281:1249–1516

Hochella MF, Liou JG, Keskinen MJ, Kim HS (1982) Synthesis and stability relations of magnesium idocrase. Econ Geol 77:798–808

Hoinkes G (1986) Effect of grossular-content in garnet on the partitioning of Fe and Mg between garnet and biotite. Contrib Mineral Petrol 92:393–399

Holloway JR (1977) Fugacity and activity of molecular species in supercritical fluids. In: Fraser DG (ed) Thermodynamics in geology. Reidel, Dordrecht, Netherlands, pp 161–181

Holloway JR (1981) Compositions and volumes of supercritical fluids in the Earth's crust. In: Hollister LS, Crawford ML (eds) Fluid inclusions: applications to petrology. Mineral. Association of Canada, Toronto, pp 13–38

Indares A, Martignole J (1985) Biotite-garnet geothermometry in the granulite facies: the influence of Ti and Al in biotite. Am Mineral 70:272–278

Jackson KJ, Helgeson HC (1985) Chemical and thermodynamic constraints on hydrothermal transport and deposition of tin: I. Calculation of the solubility of cassiterite at high pressures and temperatures. Geochim Cosmochim Acta 49:1–22

Kerrick DM, Jacobs GK (1981) A modified Redlich-Kwong equation for H_2O, CO_2 and H_2O–CO_2 mixtures at elevated pressures and temperatures. Am J Sci 281:735–767

Kreulen R, Schuiling RD (1982) N_2-CH_4-CO_2 fluids during formation of the Dôme de l'Agout, France. Geochim Cosmochim Acta 46:193–203

Kirkwood J (1939) The dielectric polarizability of polar liquids. J Chem Physics 7:911–919

Latimer WM, Pitzer KS, Slonsky CM (1939) The free energy of hydratation of gaseous ions and the absolute potential of the normal calomel electrode. J Chem Physics 7:108–111

Looyenga H (1965) Dielectric constant of heterogeneous mixtures. Physica 31:401–406

Marshall WL, Franck EU (1981) Ion product of water substance, 0–1000 °C, 1–10000 bars. New international formulation and its background. J Phys Chem Ref. Data 10:295–304

Newton RC, Wood RJ, Kleppa OJ (1981) Thermochemistry of the high structural state plagioclases. Bull Minéral 104: 162–171

Oelkers EH, Helgeson HC (1990) Triple-ion anions and polynuclear complexing in supercritical electrolyte solutions. Geochim Cosmochim Acta 54:727–738

Oelkers EH, Helgeson HC, (1992) Calculation of dissociation constants and the relative stabilities of polynuclear clusters of 1:1 electrolytes in hydrothermal solutions at supercritical pressures and temperatures. Geochim Cosmochim Acta (in press)

Perchuk LL, Lavrenteva IV (1983) Experimental investigation of exchange equilibria in the system codierite-garnet-biotite. In: Saxena SK (ed) Kinetics and equilibrium in mineral reactions. Springer, Berlin Heidelberg New York

Pitzer KJ (1983) Dielectric constant of water at very high temperature and pressure. Proc Nat Acad Sci USA, 80:4575–4576

Plimer IR (1980) Exhalative Sn and W deposits associated with mafic volcanism as precursors to Sn and W deposits associated with granites. Miner Deposita 15:275–289

Plimer IR (1987) The association of tourmaline with stratiform scheelite deposits. Miner Deposita 22:282–291

Powell R (1978) Equilibrium thermodynamics in petrology. An introduction. Harper and Row, London

Quist AS, Marshall WL (1966) Electrical conductances of aqueous solutions at high temperatures and pressures. III. The conductances of potassium bisulphate solutions from 0 to 700 °C and at pressures to 4000 bar. J Phys Chem 70, 3714–3725

Quist AS, Marshall WL (1968) Electrical conductances of aqueous sodium chloride solutions from 0 to 800 °C and at pressures to 4000 bar. J Phys Chem 72:684–703

Quist AS, Marshall WL, Jolley HR (1965) Electrical conductances of aqueous solutions at high temperatures and pressure. II. The conductances and ionization constants of sulfuric acid-water solution from 0 to 800 °C and pressures up to 4000 bar J. Phys Chem 69: 2726–2735

Rafal'skiy RP, Bryzgalin OV, Fedorov PL (1984) Tungsten migration and scheelite deposition under hydrothermal conditions. Geochem Intern 5:611–624

Ririe GT (1989) Evaporites and strata-bound tungsten mineralization. Geology 17:136–143

Schott J, Dandurand JL (1987) Prediction of the thermodynamic behavior of aqueous silica in aqueous complex solutions at various temperatures. In: Helgeson HC (ed) Chemical transport in metasomatic processes. D. Reidel, Dordrecht, Netherlands, pp 733–754

Shock EL, Helgeson HC (1988) Calculation of the thermodynamic and transport properties of aqueous species at high pressures and temperatures: correlation algorithms for ionic species and equation of state predictions to 5 kb and 1000 °C. Geochim Cosmochim Acta 52:2009–2036

Sverjensky DA, Hemley JJ, D'Angelo WM (1991) Thermodynamic assessment of hydrothermal alkali feldspar-mica-aluminosilicate equilibria. Geochim Cosmochim Acta 55:989–1004

Tweto O (1960) Scheelite in the Precambrian gneisses of Colorado. Econ Geol 55:1406–1428

Thoral M (1935) Contribution à l'étude géologique des Monts de Lacaune et des terrains cambriens et ordoviciens de la Montagne Noire. Bull Carte Géol Fr T. 38, N°192

Walther JV, Schott J (1988) The dielectric constant approach to speciation and ion pairing at high temperature and pressure. Nature 332:635–638

Wesolowski D, Drummond SE, Mesmer RE, Ohmoto H (1984) Hydrolysis equilibria of tungsten (VI) in aqueous sodium chloride solutions to 300 °C. Inorg Chem. 23:1120–1132

Wood SA, Vlassopoulos D (1989) Experimental determination of the hydrothermal solubility and speciation of tungsten at 500 °C and 1 kb. Geochim Cosmochim Acta 55:303–312

Woodland AB, Walther JW (1987) Experimental determination of the solubility of the assemblage paragonite, albite and quartz in supercritical H_2O. Geochim Cosmochim Acta 51:365–372

Zahm A (1987) The compositional evolution of calc silicates from the Salau skarn deposit (Ariège, Pyrénées). Bull Mineral 110:623–632

Editorial responsibility: J. Touret